ABSTRACT

Understanding Interactions of Glyoxal and Acetone at Aqueous and Ice Interfaces Using Vibrational Sum-Frequency Generation Spectroscopy

Camilla J. Checinski, M.S.

Mentor: Jenée D. Cyran, Ph.D.

Persistent organic pollutants, particularly volatile organic compounds (VOCs) are common contaminants in the environment that undergo long range transport and are introduced into regions where they were not previously found. Glyoxal is well-studied and one of the most abundant oxygenated VOCs in the atmosphere, produced by the oxidation of aromatic hydrocarbons in the atmosphere and through isoprene and terpene reactions. Vibrational Sum-Frequency Generation (SFG) Spectroscopy and Attenuated Total Reflection (ATR) Fourier-Transform Infrared Spectroscopy have been utilized to obtain data of free OH and CH stretch vibrational bonds at the surface and in bulk for glyoxal and acetone in aqueous solution and on ice. Glyoxal can be studied using SFG to gain an understanding of the molecular structure and orientation on the surface of ice and water. Investigating molecular level details of glyoxal on aqueous interfaces can provide information for climate models and the impact of organic pollutants on the environment.

Understanding Interactions of Glyoxal and Acetone at Aqueous and Ice Interfaces Using Vibrational Sum Frequency Generation Spectroscopy

by

Camilla J. Checinski, B.S.

A Thesis

Approved by the Department of Chemistry and Biochemistry

_____

John L. Wood, Ph.D., Chairperson

Submitted to the Graduate Faculty of
Baylor University in Partial Fulfillment of the
Requirements for the Degree
of

Master of Science

Approved by the Thesis Committee

_____

Jenée D. Cyran, Ph.D., Chairperson

_____

Bryan F. Shaw, Ph.D.

_____

Elyssia Gallagher, Ph.D.

_____

Darrin J. Bellert, Ph.D.

_____

Yang Li, Ph.D.

Accepted by the Graduate School

August 2022

_____

J. Larry Lyon, Ph.D., Dean

Page bearing signatures is kept on file in the Graduate School.

TABLE OF CONTENTS

LIST OF FIGURES

LIST OF TABLES

ABBREVIATIONS

Secondary Organic Aerosol	SOA
Volatile Organic Compound	VOC
Sum Frequency Generation	SFG
Attenuated Total Reflection	ATR
Nuclear Magnetic Resonance	NMR

ACKNOWLEDGMENTS

To my parents and brother. Thank you for your love and support and providing me with the opportunities that have led me to where I am now.

Thank you to all my friends, who have been my rock. I cannot thank you enough for your constant support, unwavering love, and believing in me when I didn't believe in myself.

I want to thank my lab mates in the Cyran Lab, it was an honor and a pleasure working with all of you. Thank you for being there to brainstorm and problem solve, especially during the long laser weeks, you kept me sane. I cannot wait to see all the great things you all complete.

To my former mentors, Dr. Jonathan Credo and Andee Lister. I cannot thank you enough for the invaluable lessons and experiences you have given me. You both taught me what a mentor and scientist should be. I want to especially thank Dr. Jani Ingram who not only provided me with an opportunity to join her group but helped me fall in love with chemistry and research. Thank you for ensuring the success of my undergraduate career and making me realize everything I was capable of accomplishing. You are a constant inspiration and role model. I would not be the scientist I am without your support.

I would like to thank the staff at Baylor University and within the Chemistry Department. Thank you Ms. Barbara Rauls for always bringing a smile to my face and Emily Jessup for all the guidance. I would like to thank Jerry Milner and Joe McCulloch

for their work on Cyran Lab projects, my research would not be possible without your expertise and skills.

To my committee members, Dr. Bryan Shaw, Dr. Elyssia Gallagher, Dr. Darrin Bellert, and Dr. Yang Li: thank you for time and serving on my committee.

Lastly, I would like to thank my advisor, Dr. Jenée Cyran, for being a great mentor. You have fostered an environment where I could thrive and provided me with so many opportunities I would not have dreamed of. I have learned so much from my time with you, not only as a student and researcher, but as an individual. Thank you for everything, I am eternally grateful.

CHAPTER ONE

Introduction

Ice and Water in the Environment

Water and ice are essential to life, not only to sustain living organisms, but to the climate and physicochemical processes within the environment.[1,2] Despite water's key role in many biological processes and its abundance in the environment, many properties of water are still not adequately understood. Phase transitions and reactions containing water molecules are some of the most important processes in the environment and are essential to understand to better study binding, adsorption, and reactions with pollutants in the environment.[1–5]

Atmospheric pollutants can be introduced into the environment through long range transport and the water cycle; these pollutants can interact with aqueous and ice surfaces, altering the properties.[1] The water and ice surface provides simple interfaces to study and utilize as model systems to better understand processes and interactions occurring at water and ice surfaces in the environment. Studying the surface elucidates questions about the degree of impact different species and conditions have on the hydrogen bond network of water and ice and provide a comparison to bulk reactions. The structure and dynamics of water can be impacted by hydrogen bond presence and cause reorientation and change the hydrogen bond strength between other water molecules.[6] These affects are important to consider because physical properties of the water surface can differ from bulk water.[6] The properties of interfacial water become especially

important to understand atmospheric aerosol surface chemistry and the impact the aerosols have in the environment on ice and water.

The structure of water and ice as interfaces and as sites for reaction mechanisms are yet to be understood comprehensively at a molecular level. Water and ice can act as sinks for organic pollutants and be revolatilized into the atmosphere.[1,7] Organic pollutants can also concentrate in ice clouds and act as sites for atmospheric reactions.[1,5]

Organic Pollutants

Airborne chemicals and pollutants can concentrate in ice clouds, acting as sites for atmospheric reactions. Once pollutants are introduced into the environment, they can undergo long range transport, where they can be carried by bodies of water and wind, and be introduced into regions where those compounds are not typically found.[1]

Atmospheric aerosols play a prominent role in the climate because they impact the balance of energy incoming and outgoing from the earth by scattering, reflecting, and absorbing sunlight.[8] The aerosols in the atmosphere can even act as nucleation sites for water and ice clouds.[8] The effects of atmospheric aerosols are dependent on the chemical and physical properties and phase state.[8] However, many properties are unknown for more atmospheric aerosols, making it difficult to understand various species interactions and reactions with water, ice, and other species.

Secondary Organic Aerosols

Atmospheric aerosols are major contributors that influence air quality, human health, and the climate. Particulate matter that is comprised of various organic species

which have underwent atmospheric transformation, is identified as secondary organic aerosols (SOA).[9–11]

Previous literature has shown that the presence of molecules at aerosol surfaces has largely influenced the atmospheric chemistry and SOA properties of these aerosols.[11–13] The increased surface area to volume ratio at the aerosol interface provides greater opportunities for these molecules to alter aerosol behavior. A majority of SOA formation mechanisms only take into account gas phase oxidation of atmospheric organic precursors, not accounting for the contribution of aqueous phase processing of atmospheric organics to SOA formation.[14] Water soluble organics, such as glyoxal, have been shown to be significant contributors to SOA formation.[15,16]

Glyoxal

Glyoxal has been identified as a potential source for atmospheric aerosols and SOA formation[8]. Glyoxal is present in the atmosphere in large quantities as a result of biomass burning, VOC oxidation, and isoprene and terpene reactions.[8,17]

While glyoxal is semi-volatile, it is extremely water soluble and can be taken up by clouds, fog, and aerosols in the aqueous phase.[12] Previous literature has shown that aqueous phase glyoxal reacts with water and tends to form monomer monohydrates and monomer dihydrates.[8,15–17] Semi-volatile atmospheric organics with carbonyls, like glyoxal, are ideal for aqueous SOA processing because the carbonyls can hydrate and form geminal diols.[13,14,16,18] Figure 1.1 depicts how hydrated species can undergo oxidation and oligomerization through acetal formation and aldol condensation, which can produce more highly oxygenated products or oligomers with increased molecular weights.[14,16,18] These products are less volatile and remain in the particle phase.

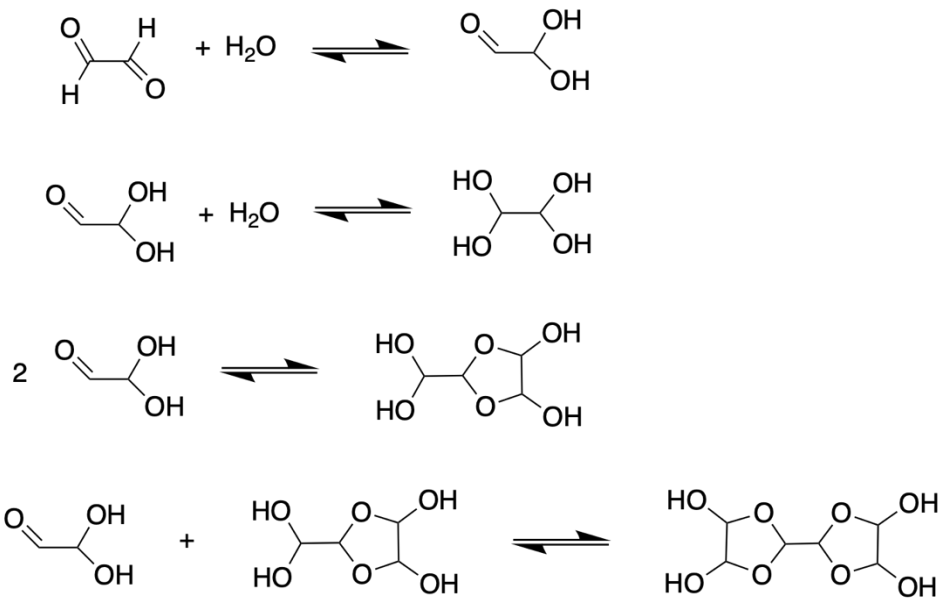

Figure 1.1. Proposed reaction equations, depicting the formation of glyoxal as a geminal diol and then reacting with itself to form dimers and trimers.

Aqueous SOA formation and processing can change atmospheric aerosol behaviors related to the climate, however those mechanisms are not adequately understood. Changing hydroscopic mass of organics can increase the particle size of atmospheric aerosols, thus impacting light scattering and cloud nucleation activity.[10,11,15] Studies have suggested that reactions can occur specifically at the surface of the aerosol. The presence of organics at the aerosol surface can decrease surface tension, influencing cloud nucleation activity.[14,19]

However, little is known about these organics on the surface and a better understanding of their interfacial behavior is needed to better predict and model their behaviors and abilities. To understand and predict the significance of aqueous SOAs, organic compound behaviors at the surface need to be characterized and identified, however, the identity, behavior, and orientation of the organic species in the environment first needs to be understood on a molecular scale.

Sum Frequency Generation

Vibrational Sum Frequency Generation (SFG) spectroscopy analyzes surfaces of molecules to investigate and provide information on molecular orientations and interactions through vibrational spectra.[20,21] SFG is a surface selective spectroscopy technique used to research vibrational states, orientations of species, bonding mechanisms at aqueous and solid interfaces.[6,22] SFG is a non-linear, second order technique where two pulsed beams, one tunable infrared (IR) and one fixed frequency visible, are spatially and temporally overlapped on a surface to generate a sum frequency signal, denoted in Eq. (1). Eq (2) expresses the electric field of SFG as the sum of two oscillating fields, ω_1 and ω_2.[20] Employing SFG spectroscopy on sample surface interfaces provides molecular scale information of only interfacial molecules, compared to linear spectroscopic techniques where the bulk signal can overwhelm the information from the interface.[23]

$$\omega_{SF} = \omega_{IR} + \omega_{VIS} \quad \text{Eq. (1)}$$

$$E = E_1 \cos \omega_1 t + E_2 \cos \omega_2 t \quad \text{Eq. (2)}$$

SFG signal produced and the energy level scheme are depicted in the schematic of Figure 1.2. SFG signal intensity is resonantly increased when the IR beam frequency is resonant with the vibrational mode of the molecules of interest.[20]

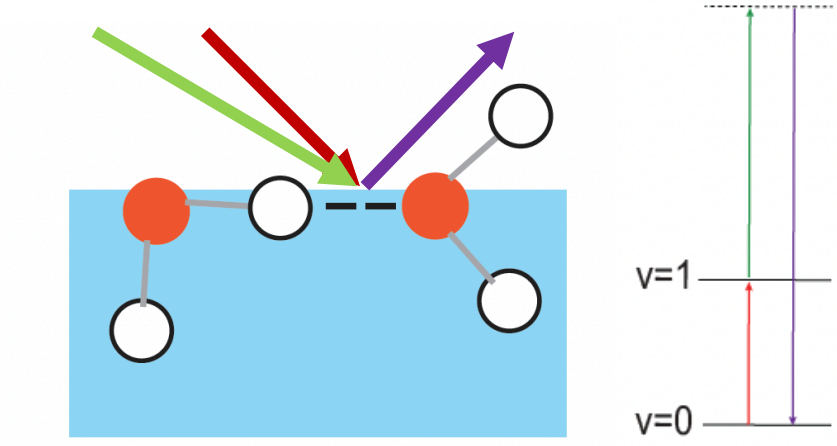

Figure 1.2. Schematic depicting the SFG generation from IR and visible beam overlap on the interface of water (left) and an energy diagram of SFG (right.

The electric field (E) of the beam induces a resultant polarization (P) (Eq. (3)).

$$P = \varepsilon_0 \chi E \qquad \text{Eq. (3)}$$

Where the linear susceptibility (χ) is described as the macroscopic average of the polarizability and where ε_0 is the vacuum permittivity.

Nonlinear effects play a significant role when the electric field is increased and second ($\chi^{(2)}$) and third ($\chi^{(3)}$) order nonlinear susceptibilities are present (Eq. (4)).

$$P = \varepsilon_0\left(\chi^{(1)}E + \chi^{(2)}E^2 + \chi^{(3)}E^3 \ldots\right) = P^1 + P^2 + P^3 \qquad \text{Eq. (4)}$$

SFG of the second order nonlinear polarization can be described in Eq. (5), where $\chi^{(2)}$ represents the second order nonlinear susceptibility (third rank tensor element), which describes that relationship between the electric field vectors of the visible and IR and the produced P vector.[20]

$$P_{SF}^{(2)} = \varepsilon_0 \chi^{(2)} E_{VIS} E_{IR} \qquad \text{Eq. (5)}$$

The produced SFG signal at the angle to surface normal (θ) can be calculated from the incoming visible and IR beams in Eq. (6).

$$n_{SF}\omega_{SF}sin\theta_{SF} = n_{VIS}\omega_{VIS}sin\theta_{VIS} \pm n_{IR}\omega_{IR}sin\theta_{IR} \quad \text{Eq. (6)}$$

Where n is the medium's refractive index, ω is the frequency, θ is the beam's angle to surface normal.

Each laser pulse, SFG, visible, and IR is polarized and denoted as S or P. The beam has an S polarization when the light has an oscillation that is perpendicular to the surface plane while P polarization is parallel to the plane. Most SFG experiments are run in SSP polarization, (SFG, visible, and IR polarization, respectively).

The frequency dependent SFG intensity (I(ω)) is proportional to the square of the effective second-order nonlinear response ($\chi^{(2)}$) and the intensities of the incident visible and IR fields in Eq. (7).

$$I(\omega_{SF}) \propto \left|\chi^{(2)}\right|^2 I_{IR}(\omega_{IR})I_{VIS}(\omega_{VIS}) \quad \text{Eq. (7)}$$

SFG's selectivity relies on second-order nonlinear optical susceptibility. To analyze the interface structure, the molecular vibrational mode must be SF active, therefore, the molecular and macroscopic levels need to be asymmetric.[20,22] SFG activity cannot be detected if molecules do not undergo emission, thus requiring the surface structure to be noncentrosymmetric and have a net polar orientation.[2] Molecules in a bulk phase with isotropic distribution are SF inactive because of their symmetry and cannot be detected using SFG. When an isotropic bulk phase interacts with an interface, an asymmetrical plane forms and the activity of interfacial molecules can be detected.[20]

This selectivity allows for SFG to provide information and vibrational spectra of the interfaces of various mediums. Surface specific orientation, bindings, and reactions can be studied to gain a better understanding of what interactions are happening at a molecular scale.

CHAPTER TWO

Methods and Materials

Single Crystalline Ice Growth

Single crystalline ice was grown using the Czochralski method using a starting seed in a solution.[24,25] A 1 inch shape cutter was used to cut a monocrystalline seed of ice that was approximately 40 mm in diameter and 10 mm deep. The ice seed was attached to a copper pin by increasing the pin temperature through a voltmeter to melt the surface of the ice when in contact with the copper. The temperature of the pin was then decreased to freeze the ice and attach it onto the copper pin. The surface layer of the ice seed is lightly melted using a heat gun and nitrogen gas to remove impurities and dust particles. The ice seed is lowered into a 0.5 ºC milliQ water bath until it is partially submerged. The water bath temperature was maintained using a Julabo F250 chiller containing a 1:1 ratio of polyethylene glycol and water to reach and maintain the desired minimum temperature. The 900 mL water bath in a crystallizing dish was surrounded by copper tubing attached to the chiller to control the temperature of the bath. A stir plate was placed beneath the crystallizing dish set to 350 rpm.

The ice seed was placed into the bath for 60 minutes at 3.0 V, after which a motor step program lifts the pin at 1.33 mm/hr with increasing voltage ever 180 min to maintain temperature of approximately 0.5 ºC throughout the duration of the growth process (Figure 2.1). The ice boules were harvested after 23 hr and placed to chill in a freezer for

30 min at -15 ºC to prevent cracking. Ice boules typically had diameters of approximately 60-70 mm and lengths of about 30 mm.

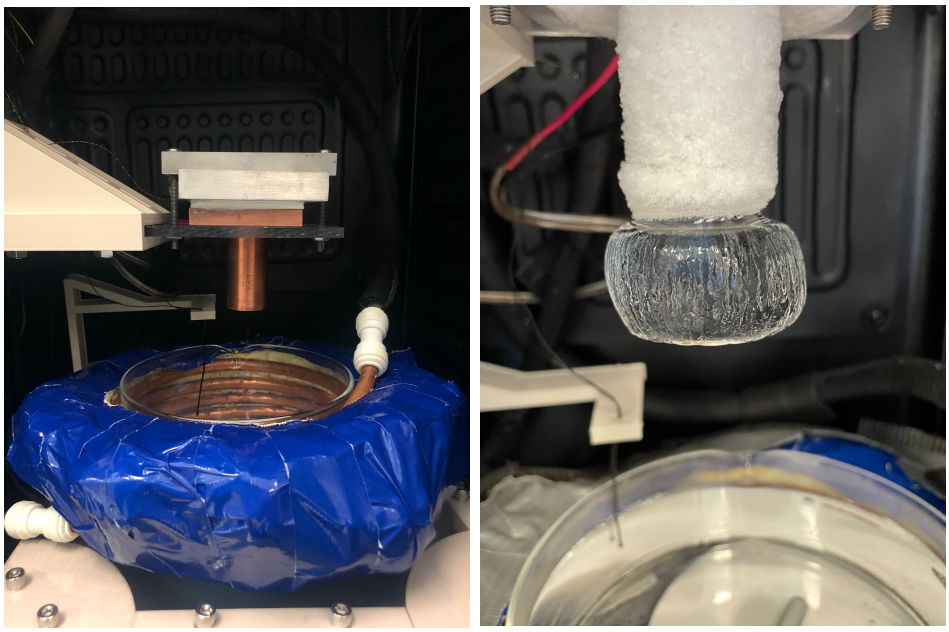

Figure 2.1. Ice growth apparatus including a crystallizing dish, surrounded by copper tubing with chiller solution to maintain ice bath temperature, including the copper pin (a). An ice growth prior to harvesting (b).

Ice boules were determined to be single or polycrystalline by using two cross polarizers. A light source was placed underneath the two polarizers which were oriented perpendicular to one another. The ice was placed between the two polarizers and the birefringence of the ice alters the outgoing light. The ice boule can appear dark when the c-axis of the ice is parallel to the incident light because light is not passing through the polarizers.[22] Polycrystalline ice can have visible domains based on the c-axis orientation of the fragment, as seen in Figure 2.2. Single crystalline ice was used for additional ice growths or for ice samples.

Figure 2.2. Images of ice boules under cross polarizers of polycrystalline ice (left) with a domain circled in red and single crystalline ice (right).

Ice Orientation

In order to use the harvested ice boules as new seeds or for spectroscopic analysis, the crystal orientation had to be determined. The orientation and face of the crystal can be determined using etching. A 2% polyvinyl formal (formvar) resin was dissolved in 1,2 dichloroethane to be used as an etching solution.[25] A chilled bandsaw was used to cut a slice of ice parallel to the seed and attached to a microscope blade using a melt-freeze method and placed in a -15 ºC freezer. The ice was microtomed using a RMT-30U Radical Scientific Equipments PVT. LTD Microtome with a Leica Triple Facet Microtome blade to create a uniform, smooth surface. The formvar solution is applied to the ice surface with a cotton swab, where the dichloroethane forms etch pits of the structure and the resin creates a thin film over the pit. The solution and water molecules evaporate through the small holes in the film, leaving behind pits that are visible through a light microscope.

The resulting images indicate the plane of the ice boule. If the orientation is not basal, as depicted in Figure 2.3, the ice boule underwent a series of cuts and reoriented to align the basal plane reference angle to the c-axis. The ice orientation procedure utilized is described in literature.[25]

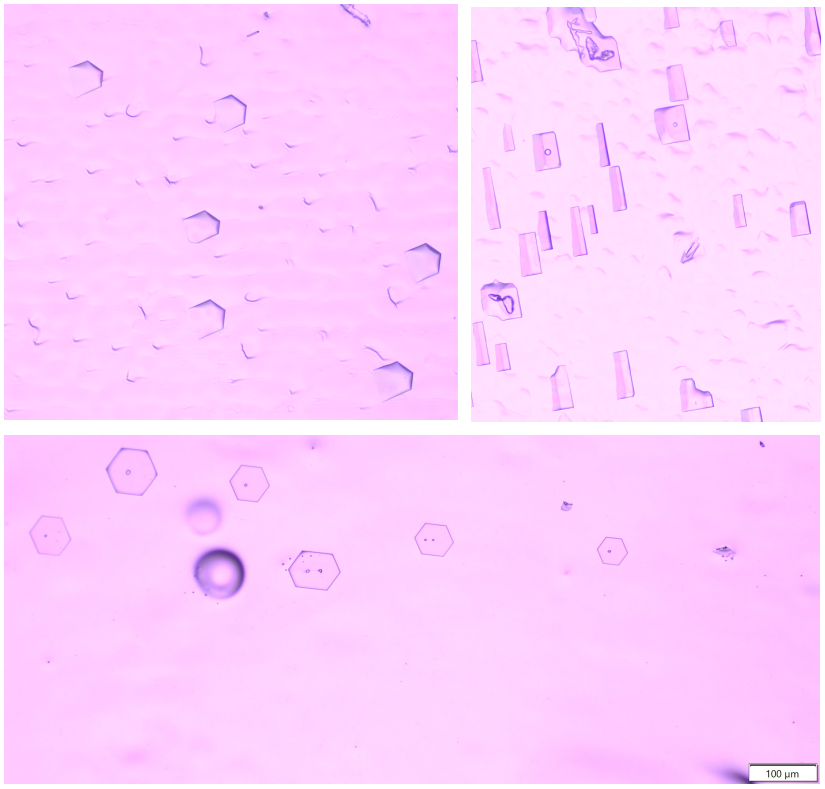

Figure 2.3. Etch pits of off axis basal plane (a), primary prism (b), and oriented basal (c) ice.

Sample Preparation

Aqueous Sample Preparation

Glyoxal, 40 w/w % aq. soln. was purchased from Alfa Aesar and HiPerSolv Chromanorm Acetone was purchased from VWR Chemicals. Glyoxal concentrations of 40% w/w (8.75 M) and 20% w/w (4.38 M) were used for aqueous sample SFG analysis using Glyoxal, 40% w/w aq. soln. from Alfa Aesar. Acetone solutions of 1 mole % (0.54

M) and 2.5 mole % (1.28 M) were prepared for analysis as a reference as other studies have quantified the adsorption of acetone on water-air and ice-air interfaces.[21] Acetone is a similarly small organic molecule, like glyoxal, and is present in the troposphere, making it atmospherically relevant to reactions in the environment. Glyoxal units were in percent w/w to be consistent with the concentration from the manufacturer. Acetone units were presented in mol % to be comparable to published acetone data.[26] Small quantities of acetone are needed to see signal on SFG, while larger quantities of glyoxal were necessary. However, molarities of each aqueous sample were included above for comparison.

Aqueous samples were collected in the flow cell depicted in Figure 2.6. A small Teflon dish is placed in the flow cell, with 3.5 mL of aqueous solution, and sealed with no nitrogen flow to avoid disturbing the aqueous surface. The aqueous samples were acquired for 5 minutes in the CH stretch region and 10 minutes in the free OH region to optimize signal intensities.

Ice Sample Preparation

Single crystalline, basal plane, ice boules were used to create the ice samples for SFG experiments. A 5 mm thick slice was cut perpendicular to the seed and a 44 mm cutter was used to produce the ice sample. A custom-made flow cell, depicted in Figure 2.4, was placed in a -15 ºC freezer and chilled until the copper reached 9 ºC. The ice sample was placed onto the copper of the flow cell and attached using the melt-freeze method. The ice in the cell chilled for 20 min prior to attaching the cell onto the microtome head. A Leica Triple Facet Microtome blade was used to shave the ice sample down to approximately 4 mm. The flow cell was then sealed and left in the freezer to

anneal for several hours (2-8 hr) prior to SFG analysis. The flow cell was placed on the cooling stage at -20 ºC, hooked up to the nitrogen flow tubing, and cooled until the stage was -50 ºC, where the ice was approximately -30 ºC. The ice cell sits on a motorized arm attached to the cooling stage and moves in circular rotations to avoid burning and melting the ice surface.

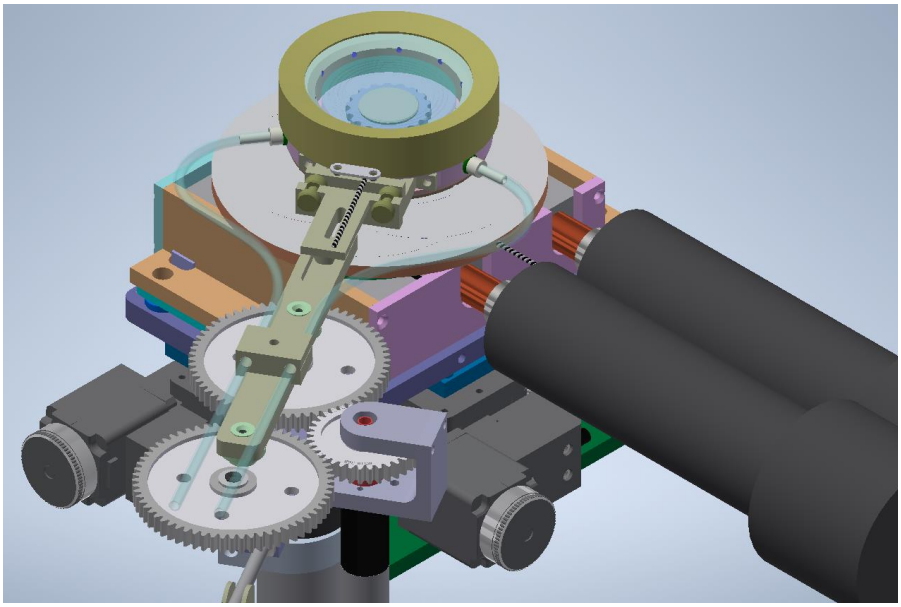

Figure 2.4. Diagram of flow cell attached to cooling stage.

Vapor Deposition

Once the ice cell was appropriately cooled, a vibrational spectrum was collected of the ice sample. Nitrogen was then flowed through the set up depicted in the schematic in Figure 2.5, over the ice for 15 minutes at 2 L/h. The tubing and flow cell set up allows the nitrogen to flow into the cell and is distributed across the surface of the ice through small ports in the cell and then exits the cell from an exit port (Figure 2.6). Nitrogen was flowed and a spectrum was collected, this process was repeated twice more to flow off

any dirt on the surface. To collect acetone deposited on the surface of ice, 50 µL of acetone was added to the gas bubbler and the nitrogen was flowed at 2 L/h at intervals, 30s, 60s, 90s, and 120s, where spectra were collected between each flow for 1 minute.[26] The same procedure was followed for glyoxal deposition on a new ice sample after the gas bubbler and tubing were cleaned using a procedure of acetone, ethanol, and water.

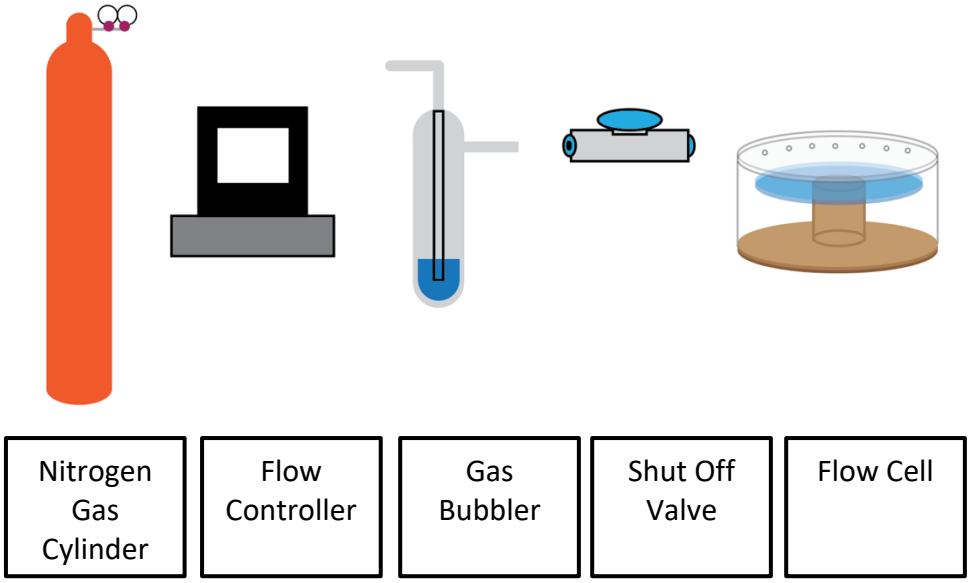

Figure 2.5. Schematic diagram of the nitrogen flow set up.

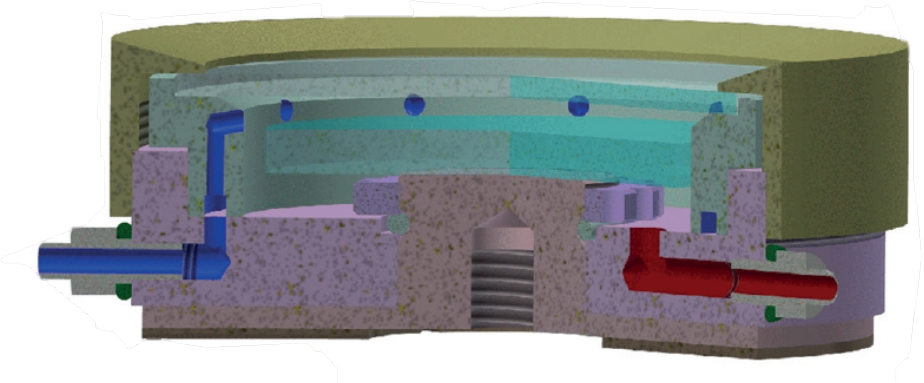

Figure 2.6. Diagram of flow cell and nitrogen flow over the ice.

Laser System

SFG spectra were collected using a sub-picosecond system. The laser system is comprised of Ti:Sapphire laser with an ultrafast regenerative amplifier (Astrella, Coherent), which produces 1kHz pulses at approximately 60 fs. The initial amplified 800 nm beam is split to an optical parametric amplifier (TOPAS Prime, Light Conversion) in tandem with a difference frequency generator (DFG) to mix and generate IR. The remainder of the visible beam is directed to the visible path and passes through an etalon that narrows the frequency to 0.5 nm. Polarizers and half-wave plates dictate the visible and IR beam powers and polarizations. The visible and IR beams were overlapped in space and time on the sample surface, where a sum frequency light was emitted. The SFG signal produced is detected with a thermoelectrically cooled CCD camera (ISOPlane160, Princeton Instruments). Aqueous samples collected at 3100 nm and 2750 nm were acquired for 300 s and 600 s respectively. Aqueous and ice samples were collected in SSP polarizations, at 15 ºC for liquid samples and -30 ºC for ice samples.

SFG Spectra Collection

Prior to collecting SFG spectra of the samples, the SFG signal was optimized using z-cut quartz, where the optic axis is perpendicular to the surface plane. Once signal is optimized, a quartz spectrum was collected for 5 and 10 seconds for aqueous and ice samples respectively. Background spectra are collected for quartz and samples by blocking the IR beam to then subtract the background from the spectra. A polystyrene spectrum was collected to correct any visible wavelength of 800nm variance by using know literature peaks of polystyrene and matching the wavenumbers when converting from wavelength to wavenumber. The collected SFG spectra for both aqueous and ice

samples were background subtracted and normalized by dividing by the reference spectrum using MATLAB.

SFG Spectra Fitting

The reference divided spectra of the samples were fit to determine the impact of concentration on the molecular interactions of glyoxal and acetone on water and ice interfaces. The peaks in the SFG spectra were fit using Lorentzian functions, described below in Eq. (8).

$$I_{VSFG} \propto \left| A_{NR} e^{i\varphi NR} + \frac{A_i}{\omega - \omega_i + i\Gamma_i} \right|^2 \quad \text{Eq. (8)}$$

A_{NR} represents the non-resonant amplitude and φ_{NR} represents the non-resonant phase. The amplitude (A_i), frequency (ω_i), and width (Γ_i) make up the resonant contribution for the vibration. Values used to fit the peaks help quantify changes in peak intensity and frequency shifts.

Attenuated Total Reflection Fourier Transform Infrared Spectroscopy

Bulk spectroscopy measurements of aqueous acetone and glyoxal samples were taken with Attenuated total reflection fourier transform infrared (ATR-FTIR) spectroscopy (Andover), to compare surface and bulk spectra. A pipet was used to deposit two drops of water, glyoxal, and acetone solutions onto the ATR crystal. The crystal was rinsed with water in between samples to prevent cross contamination.

pH Measurements

pH measurements of the aqueous samples were collected to determine if the pH changed beyond the change in concentration. Measurements were taken using a SevenExcellence pH meter S400-Bio-Kit (Mettler Toledo) at room temperature.

NMR

Nuclear Magnetic Resonance (NMR) spectra of aqueous glyoxal were obtained with an Bruker Fourier 300 MHz and a Bruker 400 MHz NMR to determine the presence of monomeric glyoxal and other glyoxal oligomers. A preliminary, small scale distillation was conducted in attempt to isolate the glyoxal from the aqueous solution. Chloroform-[D_1] (99.9 atom % D, Acros Organics) was used as the solvent. Proton NMR spectra were collected of the 40 % w/w glyoxal, the distillate that was collected, and what remained in the original flask to quantify the presence and state of glyoxal. An additional Carbon NMR spectrum was collected to determine the presence of CH's in the glyoxal solution, using D_2O as a solvent for better glyoxal dispersion (Cambridge Isotope Laboratories).

CHAPTER THREE

Results

SFG Analysis of Aqueous Samples

SFG spectra of clean MilliQ water were collected to serve as comparisons to the acetone and glyoxal aqueous samples. The water spectra for both the free OH and CH stretch regions are depicted in Figure 3.1. The bonded OH is visible at 3100 – 3500 cm^{-1} while the free OH peak at the interface is seen at 3750 cm^{-1}. In Figure 3.1b there is an example of a CH peak from acetone which would be found approximately at 2950 cm^{-1}.

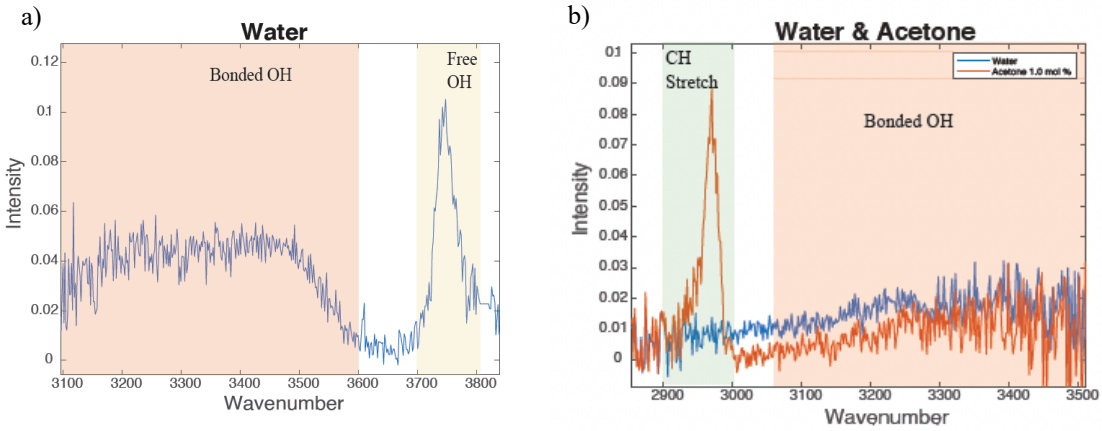

Figure 3.1. Vibrational SFG spectra of water in free OH (a) and CH stretch region (b).

Vibrational spectra of aqueous acetone samples of 1 mole % and 2.5 mol % concentrations are shown in Figure 3.2. Changes in peak intensity, frequency, and width were quantified with Lorentzian fits displayed in Table 3.1. The sharp free OH peak of water decreases in intensity with the presence of acetone, indicating that there are less free OH's available at the surface. This is conclusive with previous literature that

suggested acetone prefers to interact with the free OH groups available at the surface1. A shift in the bonded OH region of the acetone samples is seen in Figure 3.2 to a higher frequency, suggesting that the surface hydrogen bonds are weakening with the addition of acetone.

A similar trend to acetone is seen in the free OH peak of the glyoxal samples, where the free OH signal decreases in intensity as the glyoxal concentration is increased, suggesting that less free OH groups are available at the surface (Figure 3.2). A shift in frequency for the bonded OH band is observed with the presence of acetone, as noted by the change in the Peak 2 frequency in Table 3.1. An increase in frequency in the bonded OH peak is attributed to the distance between oxygen atoms, which increases with the presence of acetone, weakening the bonds.[26] However, there is not a shift in the bonded OH as with acetone in the aqueous glyoxal samples in either Figure 3.2d or 3.2e, which suggests that the interaction between the glyoxal molecules differs from the interaction between acetone and water. The shift in the bonded OH band in acetone has been attributed to the interaction between the oxygen of acetone's carbonyl and the free OH.[26] If glyoxal has already formed oligomers or has diol moieties, then the same frequency shift would not occur because the interaction of the carbonyl is not available.

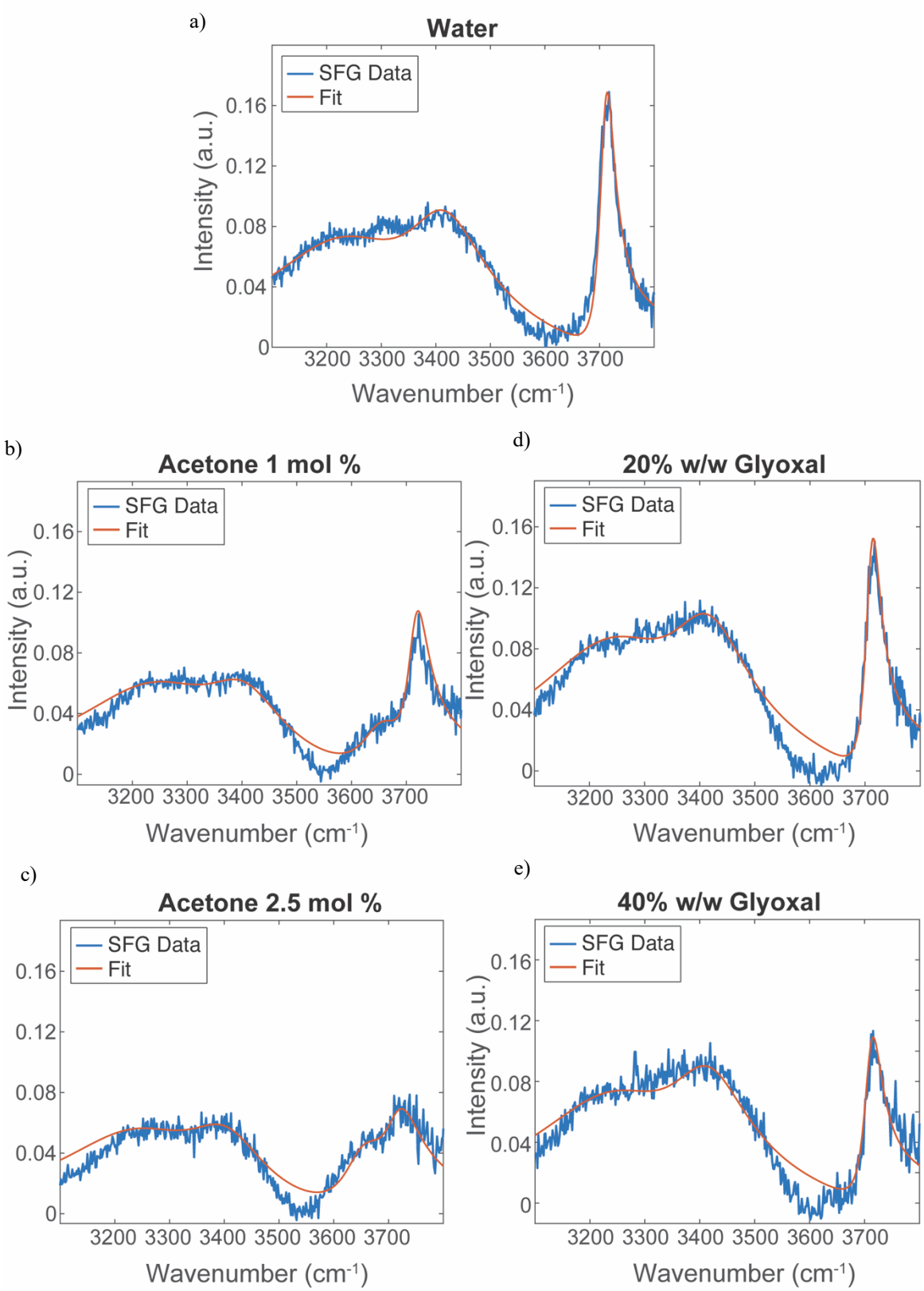

Figure 3.2. SFG spectra of water (a), acetone 1 mol % (b), acetone 2.5 mol %(c), glyoxal 20 % w/w (d), and glyoxal 40 % w/w (e), solutions in the free OH region (blue) with fitting (red).

Table 3.1. Fitting parameters for SFG Spectra in Figure 3.2. Parameters for peaks not present in certain samples are denoted with '-'.

		Samples Free OH				
Fitting Parameter		Water	Acetone (1 mol%)	Acetone (2.5 mol%)	Glyoxal (20% w/w)	Glyoxal (40% w/w)
A_{NR}				0		
φ_{NR}				0		
Peak 1	Amplitude (A_i)	-38	-34	-32	-35	-37
	Frequency (ω_i)	3250	3250	3250	3250	3250
	Width (Γ_i)	170	170	170	150	170
Peak 2	Amplitude (A_i)	-15	-12	-11	-17.5	-15.25
	Frequency (ω_i)	3410	3400	3400	3410	3410
	Width (Γ_i)	90	90	90	90	90
Peak 3	Amplitude (A_i)	-	-6.25	-6.25	-	-
	Frequency (ω_i)	-	3650	3650	-	-
	Width (Γ_i)	-	50	50	-	-
Peak 4	Amplitude (A_i)	-6.5	-3.75	-5.25	-2.65	-2.55
	Frequency (ω_i)	3710	3715	3715	-3710	3710
	Width (Γ_i)	20	20	40	17	20

Meanwhile, in the CH region SFG spectra depicted in Figure 3.3, glyoxal and acetone have different CH bands present. Table 3.2 displays the fitting parameters used to quantify the spectra peaks. In Figure 3.3a, 3.3b and Table 3.2, acetone has a sharp CH

peak seen at 2933 cm^{-1}. The glyoxal spectra in Figure 3.3c and 3.3d on the right do not have a strong CH peak, but rather two peaks at 2885 cm^{-1} and 2945 cm^{-1}. The two broad CH peaks are typically attributed to symmetric and asymmetric vibrational stretching of the CH on the surface. However, glyoxal's preference to form diols and oligomerize, the CH peaks are likely due to the presence of various CH stretches associated with rings and dimers as glyoxal oligomerizes. To determine the presence of dimers and trimers, ATR and NMR analysis were run.

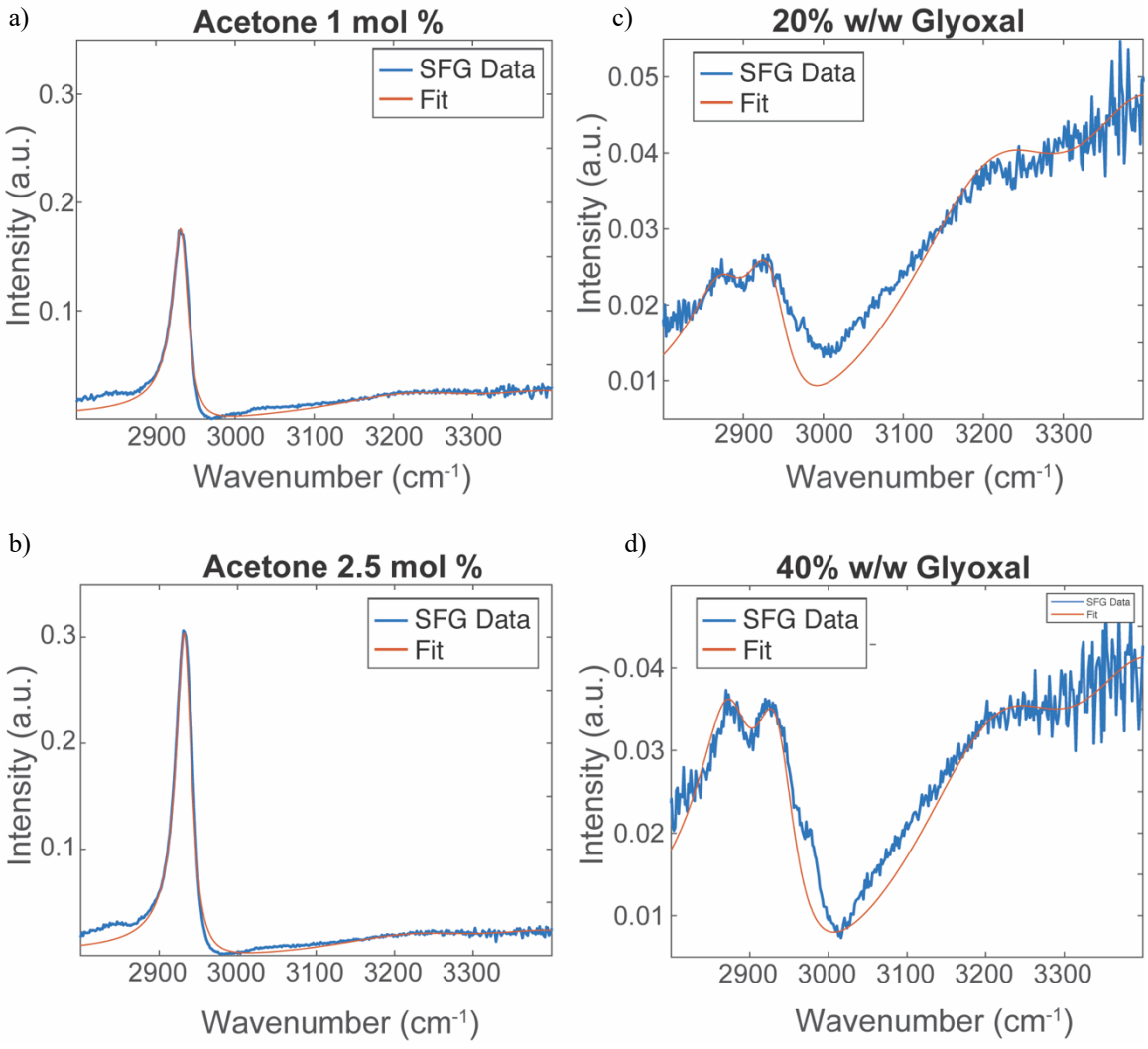

Figure 3.3. SFG spectra of acetone (a and b) and glyoxal (c and d) solutions in the CH stretch region (blue) with fitting (red).

Table 3.2. Fitting parameters for SFG Spectra in Figure 3.3.

Fitting Parameter		Samples CH Stretch				
		Water	Acetone (1 mol%)	Acetone (2.5 mol%)	Glyoxal (20% w/w)	Glyoxal (40% w/w)
A_{NR}				0		
φ_{NR}				0		
Peak 1	Amplitude (A_i)	-11.5	-12.5	-11.5	-13.75	-13.5
	Frequency (ω_i)	3220	3220	3220	3220	3165.3220
	Width (Γ_i)	130	130	130	130	130
Peak 2	Amplitude (A_i)	-25	-16	-15	-23	-21.5
	Frequency (ω_i)	3400	3400	3400	3400	3400
	Width (Γ_i)	130	130	130	130	130
Peak 3	Amplitude (A_i)	-	-4.5	-6.15	-2.25	-3.5
	Frequency (ω_i)	-	2933	2933	2945	2945
	Width (Γ_i)	-	12	12	35	35
Peak 4	Amplitude (A_i)	-	-	-	-1.5	-2.75
	Frequency (ω_i)	-	-	-	2885	2885
	Width (Γ_i)	-	-	-	34	45

SFG Analysis of Ice

Vibrational spectra of ice were collected in the CH region using the vapor flow set up and served as a reference comparison prior to the flow of acetone and glyoxal. The top row of spectra in Figure 3.4 shows clean ice. Acetone was placed into a gas bubbler and

nitrogen was used as a carrier gas to deposit acetone vapor onto the surface of ice at different deposition times. Figure 3.4e shows a spectrum collected of 20 s of acetone flow, with a CH peak visible at 2940 cm^{-1}, with the presence of some unidentified dirt at 2880 cm^{-1}. An increase in the CH peak intensity is seen in Figure 3.4f which had a longer deposition time of 90s. Increasing the deposition allowed for more CH groups to cover the ice surface, thus increasing the CH intensity.

Figure 3.4a-c represents the vibrational spectra collected of clean ice and glyoxal flowed on ice. However, there does not appear to be any formation of CH peaks visible in Figure 3.4b and 3.4c, which had 30s and 90s of glyoxal vapor deposition respectively. The lack of CH peaks indicates that glyoxal is not present or interacting on the ice surface. If dimers and trimers of glyoxal are present in the solution, a higher flow rate would be required to deposit the glyoxal molecules because the molecular mass is increased. Simulations done by Hudait et al. of glyoxal and ions on the ice surface have determined that glyoxal molecules do not experience water driven attraction to the "liquid like" water molecules on the surface of ice and are instead attracted to other ions and glyoxal molecules, therefore on ice surfaces the simulation revealed that glyoxal accumulates in dry clusters.[27] However, experimental results do not observe any glyoxal interaction on the ice surface in the CH region. Additional experiments and time intervals were run for glyoxal to determine if increasing deposition time increases. There was no visible CH peak present on ice at 120s and 360s glyoxal flow times. Experimental parameters need to be expanded and tested to evaluate glyoxal's interactions on interfacial ice. Additional spectra should be collected in the free OH region to determine if any changes in the free OH peak are detected.

Uncertainties and errors in ice preparation could contribute to variances seen in the collected ice data. Basal ice boules are harvested from basal seeds, the most common discrepancy occurs in the degree that the plane is off axis, however that can be corrected utilizing a series of cuts to account for the angle. Single crystalline, basal oriented ice, with an error of $< 5^{o}$ off axis was utilized for SFG analysis. Despite the potential difference in angles between ice used for analysis, the small degree of variance should not impact the available free OH at the surface.

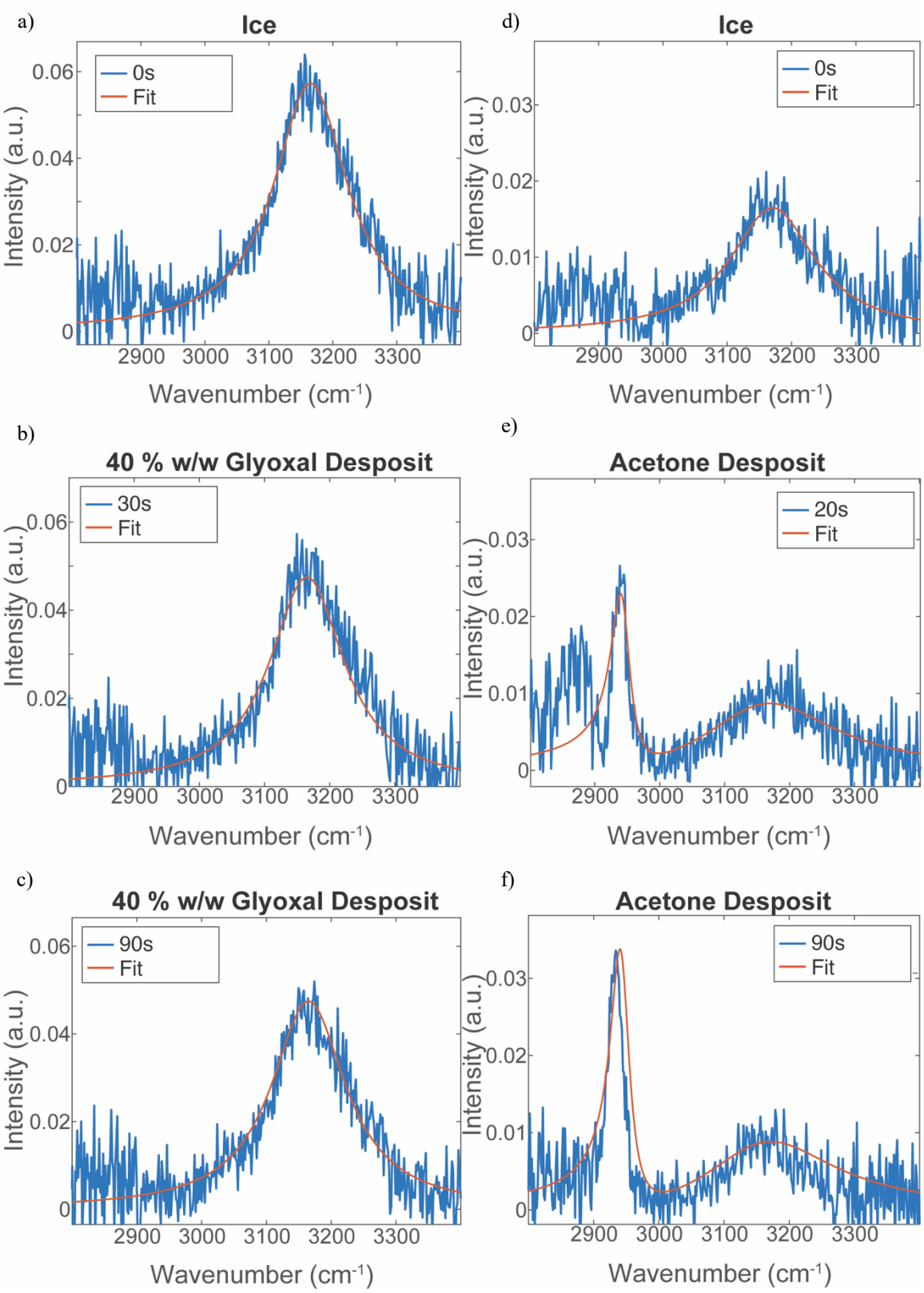

Figure 3.4. SFG spectra of glyoxal vapor deposition on ice for 0s (a), 30s, (b), and 90s (c) and acetone vapor deposition on ice for 0s (d), 20s (e), and 90s (f) in the CH stretch region (blue) with fitting (red).

Table 3.3. Fitting parameters for SFG Spectra in Figure 3.4.

		Samples					
Fitting Parameters		Ice (a)	Glyoxal (30s)	Glyoxal (90s)	Ice (d)	Acetone (20s)	Acetone (90s)
A_{NR}				0			
φ_{NR}				0			
Peak 1	Amplitude (A_i)	-16.5	-15.75	-15.0	-10.75	-7.75	-7.5
	Frequency (ω_i)	3165	3165	3165	3165	3165	3165
	Width (Γ_i)	70	70	70	80	80	80
Peak 2	Amplitude (A_i)	-	-	-	-	-2.4	-2.75
	Frequency (ω_i)	-	-	-	-	2945	2937
	Width (Γ_i)	-	-	-	-	17	17

ATR Analysis

ATR analysis was conducted to compare bulk signal to surface SFG spectra to confirm glyoxal oligomers were present in the aqueous solution. The ATR spectra collected, shown in Figure 3.5, aligns with FTIR data collected by Avzianova et al., where multiple peaks in the 900 to 1200 cm^{-1} region match peaks in literature attributed to ring stretching, indicating that some glyoxal oligomers have formed in the aqueous solution.2 The data in Figure 3.5 also matches ATR-IR spectra collected by Peters et al. of 40 wt % and 4 wt % of aqueous glyoxal, who identified the peak maxima's at 1053, 997, and 948 cm^{-1} as dimers and other oligomers, but due to the molecular similarity between the groups it is difficult to assign specific bands to each species.3 However, the ATR data collected in Figure 3.5 does indicate the presence of dimers and trimers in

solution as depicted by the presence of the peaks at 1060, 998, and 950 cm^{-1} that correspond to CO bonds and moieties attributed to ring structures.

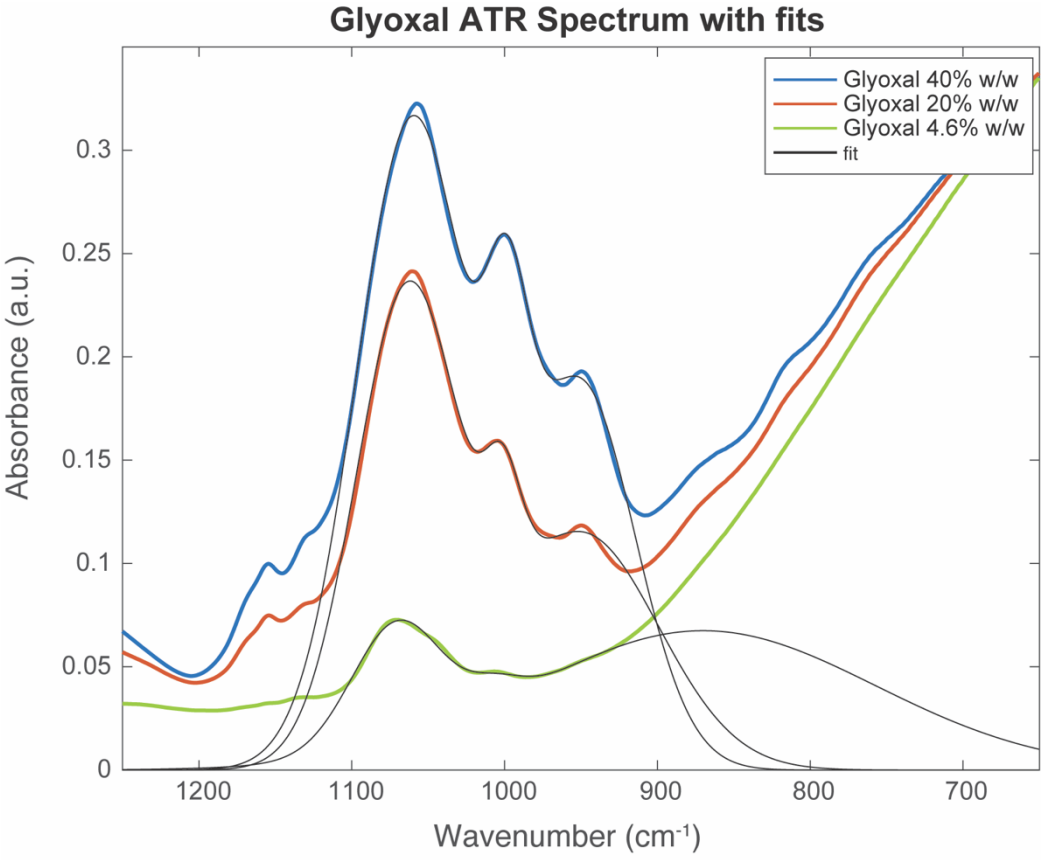

Figure 3.5. ATR spectra collected of water (blue), 40 w/w% glyoxal (red), 20 w/w% glyoxal (yellow), and 4.6 w/w % glyoxal (green), with fits (black).

ATR Fitting

The ATR spectra in Figure 3.5 were fit with Lorentzian peak parameters listed in Table 3.4. The Lorentzian equation below for 3 peaks was used to fit the three maxima between 900 and 1100 cm^{-1} in Figure 3.5 in order to determine the peak positions and compare the values to previous literature to identify the peaks.

$$f(x) = a1^{(-(x-b1/c1)^2)} + a2^{(-(x-b2/c2)^2)} + a3^{(-(x-b3/c3)^2)} \quad \text{Eq. (9)}$$

The parameters describe the peak amplitude, frequency, and width. The peak maxima's used for the fitting in Table 3.4 below matched closely to the literature values presented by Peters et al. for the 40 w/w % glyoxal solution: 1060, 998, and 950 cm^{-1}. The peaks signify the presence of CO stretching associated with rings, suggesting that dimers and trimers have already formed in solution.

Table 3.4. Fitting parameters for Figure 3.5.

		Glyoxal Sample		
Peak	Parameter	40 w/w %	20 w/w %	4.6 w/w %
	a1	0.3149	0.2270	0.0583
1	b1	1060	1064	1071
	c1	52.57	47.98	41.85
	a2	0.104	0.0480	0.0674
2	b2	998.4	1001	870.1
	c2	19.97	16.69	159.4
	a3	0.1857	0.1146	0.0089
3	b3	950.4	950.0	1006
	c3	51.00	71.86	25.00

pH Measurements

The collected pH measurements of the aqueous samples are listed in Table 3.5 below. The glyoxal pH values change in proportion to the change in concentration. Glyoxal is a strong acid and therefore the pka is low at -7.8. Even at lower concentrations such as 4.6 ww %, the equivalent of 1 M, the glyoxal solution is acidic. The low pH of organics in the atmosphere can alter the formation and growth of clouds and the pH of rainwater.

Table 3.5. Average pH and standard deviation for aqueous samples.

Sample	pH Average	Standard Deviation
MilliQ	7.326	0.005
Glyoxal 40 w/w %	1.950	0.004
Glyoxal 20 w/w %	2.354	0.007
Glyoxal 4.6 w/w %	2.906	0.006
Acetone 1.0 mol %	6.997	0.062
Acetone 2.5 mol %	6.790	0.002

NMR

A small scale distillation was set up using a water condenser and vacuum pump to attempt to isolate glyoxal from the aqueous solution, however glyoxal's volatility makes this approach difficult. A small solution of the collected distillate was ran to determine if there was any glyoxal isolated. The proton NMR spectra of 40 % w/w glyoxal solution (Figure 3.6), collected distillate (Figure 3.7), and remainder of starting flask (Figure 3.8), each have water and chloroform-D present at 1.5 ppm and 7.2 ppm, respectively. If monomers of glyoxal were present, a chemical shift would be present around 9-10 ppm, however chemical shifts attributed to aldehydes are not present in the original solution. Figure 3.6 does have chemical shifts between 4.5 and 5.2 ppm, which could be associated with the presence of diols. Chemical shifts in Figure 3.7 of the collected distillate are much more prominent, suggesting that the distillation was able to collect glyoxal, in its diol form. Carbon NMR of the original glyoxal solution in Figure 3.9 shows the C-O bond and the chemical shifts similar to those found in previous literature.[28] Zhang et al.

determined that the glyoxal peaks in the 90 – 110 ppm range were due to the hydrated state of glyoxal and the formation of oligomers. No aldehydes were identified in the C NMR as a chemical shift would be visible at 190-200 ppm. However, the lack of CH peaks in both H and C NMR makes it hard to determine the true CH interaction seen in the SFG vibrational spectra. Further testing and additional distillations may be attempted in order to better characterize the glyoxal solution.

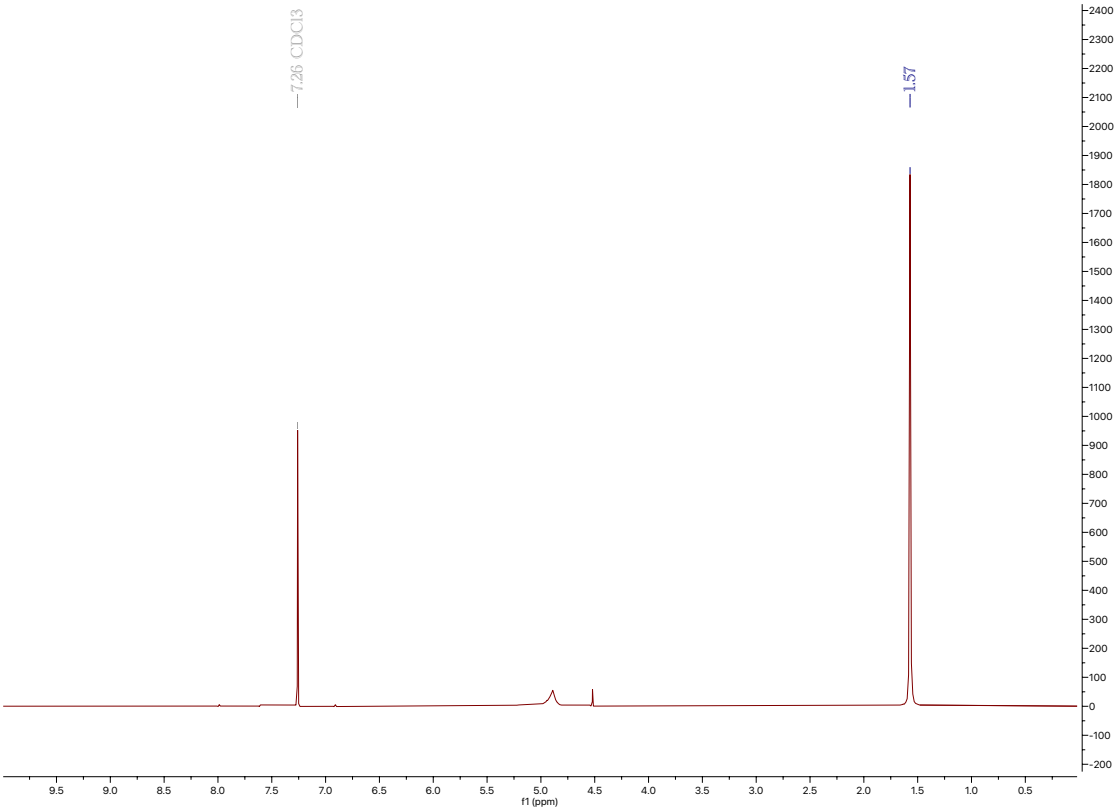

Figure 3.6. Proton NMR spectra of 40 % w/w glyoxal in aqueous solution.

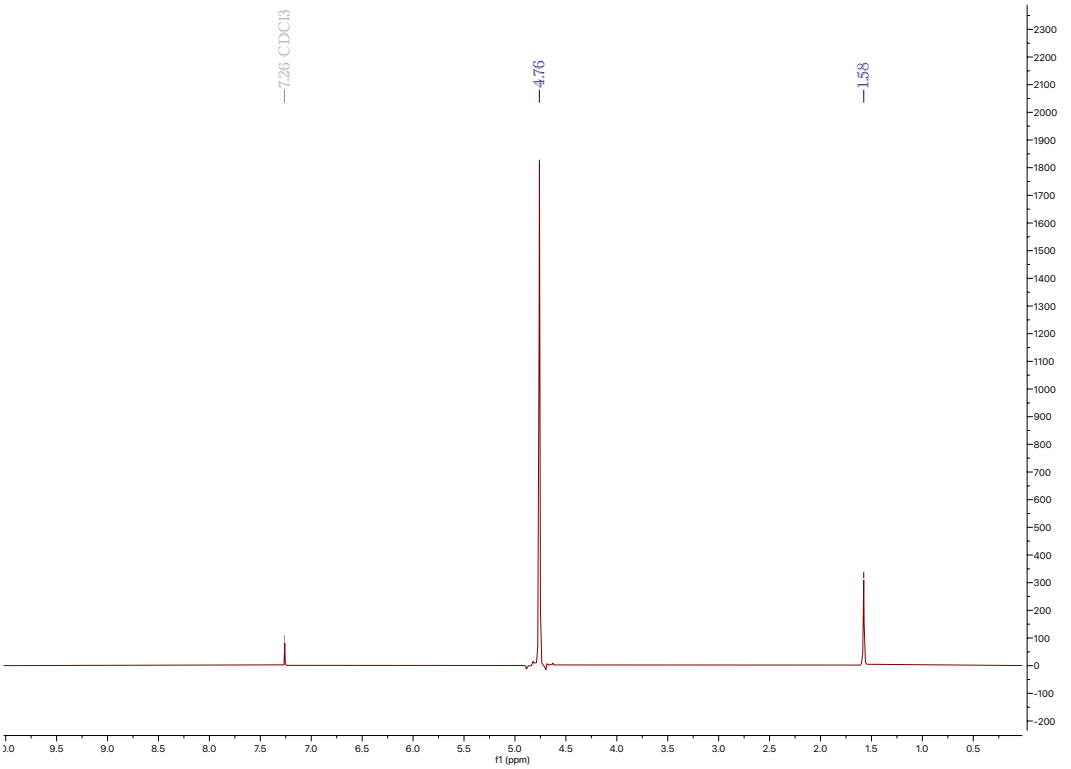

Figure 3.7. Proton NMR spectra of glyoxal distillate.

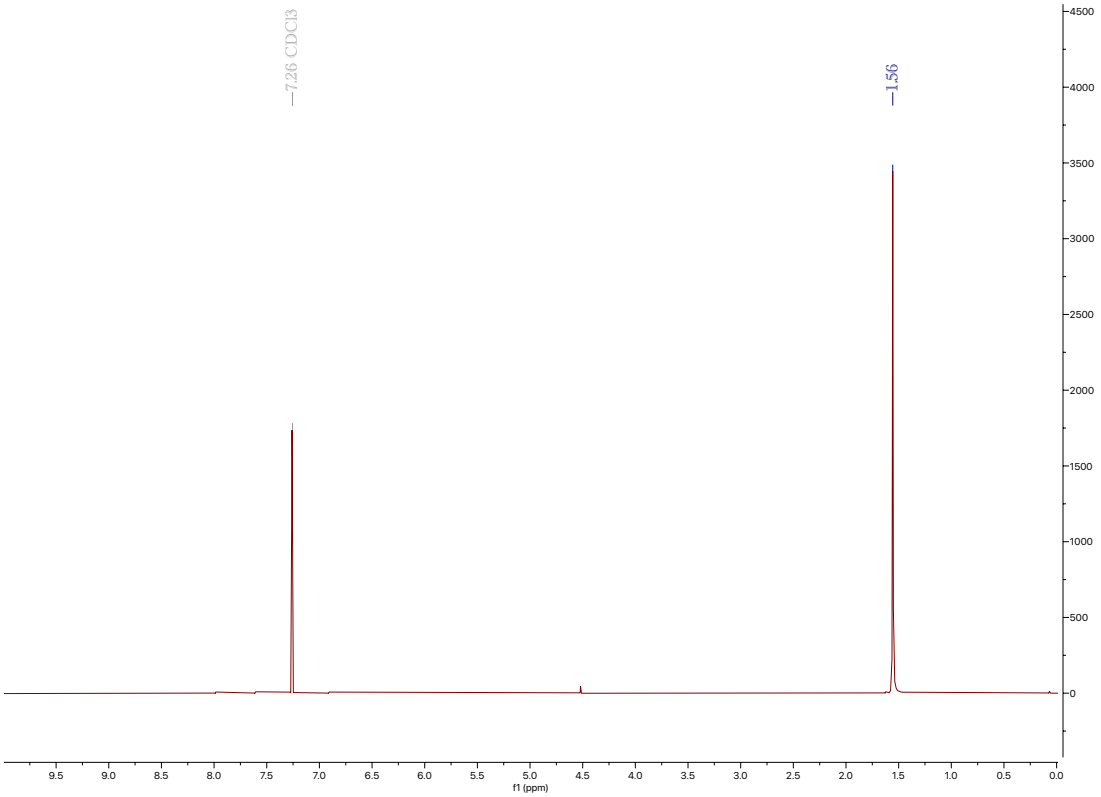

Figure 3.8. Proton NMR spectra of remaining starting material.

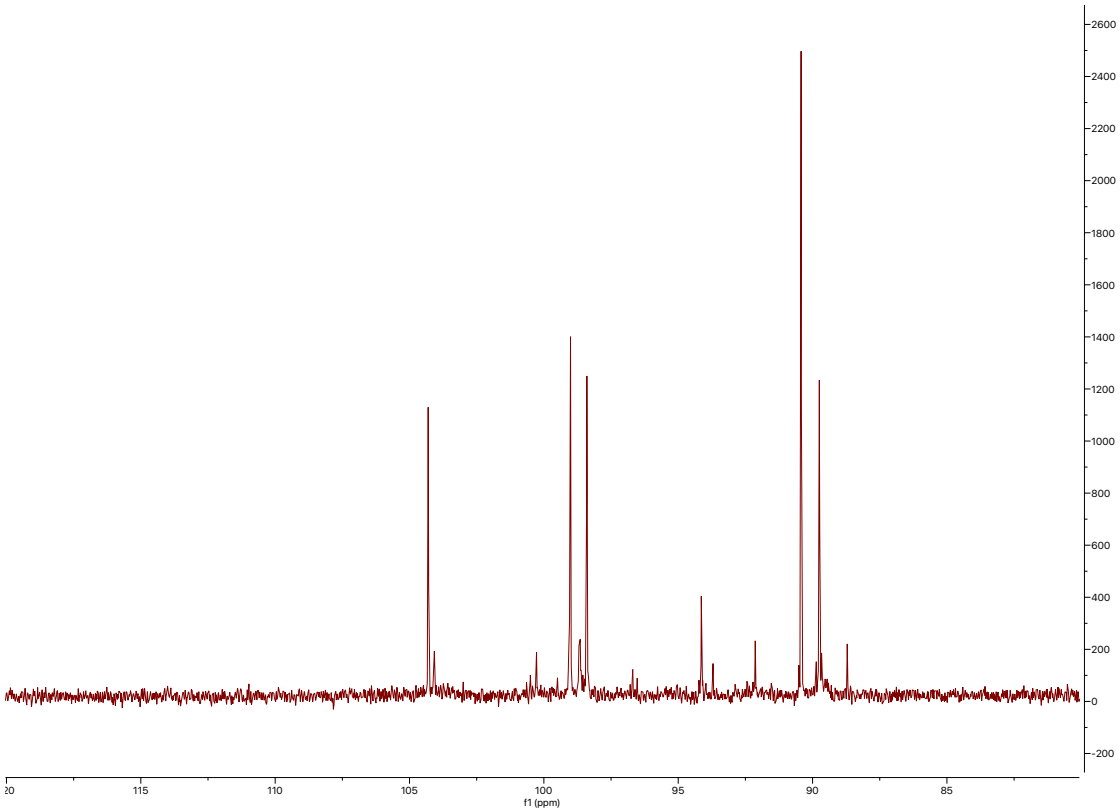

Figure 3.9. Carbon NMR spectra of 40% w/w glyoxal.

CHAPTER FOUR

Conclusion

SFG spectra of aqueous samples of glyoxal and acetone show a decrease in free OH signal with the increase of sample concentration, suggesting less free OH groups are available at the surface of water. However, acetone shows a shift in the bonded OH peak not seen in glyoxal, suggesting that glyoxal has a different interaction with interfacial water molecules than acetone. Glyoxal also has two CH peaks in aqueous solution while acetone has a singular sharp peak, indicating that there are different CH interactions between the molecules, which could be attributed to the oligomerization of glyoxal.

Initial SFG spectra that have been collected in the CH stretch region on the ice surface has shown that acetone is deposited on the surface in accordance with literature. However, glyoxal and the presence of CH peaks were not seen on the collected ice spectra. The presence of glyoxal dimers and trimers makes vapor deposition more difficult.

Glyoxal is known to form oligomers and previous studies have suggested that dimers and trimers are present in 40 % w/w glyoxal solutions. An ATR analysis matched previous literature with visible bands in the CO ring stretching region, indicating that glyoxal oligomers are forming in the bulk and likely on the surface as indicated by the CH stretch of glyoxal in the SFG spectra. The two CH peaks of glyoxal are likely the CH vibrations belonging to a dimer and trimer. However, further analysis of aqueous glyoxal will need to be completed at a polarization parallel to the surface (PPP or SPS)

polarizations to determine if glyoxal monomers are oriented at a different angle. Future work should include the collection of vibrational spectra in the carbonyl region (SSP, PPP, SPS polarizations) to determine and evaluate the presence and orientation of carbonyls in glyoxal aqueous samples.

Future work on quantifying glyoxal's interaction with the ice-air interface would be composed of additional ice spectra collection at various parameters to determine if glyoxal can be vapor deposited onto the surface of ice under optimized conditions such as increased flow. SFG Analysis in the free OH region would provide more information on the interaction of glyoxal and the free OH of ice, which can then be compared to the aqueous SFG data.

The results collected from the study can be utilized and applied to atmospheric studies. Understanding the presence and formation of dimers and trimers of glyoxal is needed to better quantify glyoxal in the atmosphere and how it interacts with different aerosols and environmental interfaces. While glyoxal seems not to be predominantly in a monomeric state at the sample concentrations analyzed in this study, atmospheric pollutants are found in much smaller concentrations in the atmosphere and therefore more monomeric glyoxal could be present and reacting with aerosols and in ice clouds. Once further studies are conducted to elucidate glyoxal's orientation and interaction with ice and water surfaces, the molecular information can be used in simulations and computational work to predict various behaviors in the environment and the impact on climate models.

REFERENCES

(1) Bartels-Rausch, T.; Bergeron, V.; Cartwright, J. H. E.; Escribano, R.; Finney, J. L.; Grothe, H.; Gutiérrez, P. J.; Haapala, J.; Kuhs, W. F.; Pettersson, J. B. C.; Price, S. D.; Sainz-Díaz, C. I.; Stokes, D. J.; Strazzulla, G.; Thomson, E. S.; Trinks, H.; Uras-Aytemiz, N. Ice Structures, Patterns, and Processes: A View across the Icefields. *Reviews of Modern Physics* **2012**, *84* (2), 885–944. https://doi.org/10.1103/RevModPhys.84.885.

(2) Tang, F.; Ohto, T.; Sun, S.; Rouxel, J. R.; Imoto, S.; Backus, E. H. G.; Mukamel, S.; Bonn, M.; Nagata, Y. Molecular Structure and Modeling of Water-Air and Ice-Air Interfaces Monitored by Sum-Frequency Generation. *Chemical Reviews*. American Chemical Society April 22, 2020, pp 3633–3667. https://doi.org/10.1021/acs.chemrev.9b00512.

(3) Arsiccio, A.; Pisano, R. The Ice-Water Interface and Protein Stability: A Review. *Journal of Pharmaceutical Sciences*. Elsevier B.V. July 1, 2020, pp 2116–2130. https://doi.org/10.1016/j.xphs.2020.03.022.

(4) Naullage, P. M.; Metya, A. K.; Molinero, V. Computationally Efficient Approach for the Identification of Ice-Binding Surfaces and How They Bind Ice. *Journal of Chemical Physics* **2020**, *153* (17). https://doi.org/10.1063/5.0021631.

(5) McNeill, V. F.; Grannas, A. M.; Abbatt, J. P. D.; Ammann, M.; Ariya, P.; Bartels-Rausch, T.; Domine, F.; Donaldson, D. J.; Guzman, M. I.; Heger, D.; Kahan, T. F.; Klán, P.; Masclin, S.; Toubin, C.; Voisin, D. Organics in Environmental Ices: Sources, Chemistry, and Impacts. *Atmospheric Chemistry and Physics*. 2012, pp 9653–9678. https://doi.org/10.5194/acp-12-9653-2012.

(6) Bonn, M.; Nagata, Y.; Backus, E. H. G. Molecular Structure and Dynamics of Water at the Water–Air Interface Studied with Surface-Specific Vibrational Spectroscopy. *Angewandte Chemie* **2015**, *127* (19), 5652–5669. https://doi.org/10.1002/ange.201411188.

(7) Bartels-Rausch, T.; Jacobi, H. W.; Kahan, T. F.; Thomas, J. L.; Thomson, E. S.; Abbatt, J. P. D.; Ammann, M.; Blackford, J. R.; Bluhm, H.; Boxe, C.; Domine, F.; Frey, M. M.; Gladich, I.; Guzmán, M. I.; Heger, D.; Huthwelker, T.; Klán, P.; Kuhs, W. F.; Kuo, M. H.; Maus, S.; Moussa, S. G.; McNeill, V. F.; Newberg, J. T.; Pettersson, J. B. C.; Roeselová, M.; Sodeau, J. R. A Review of Air-Ice Chemical and Physical Interactions (AICI): Liquids, Quasi-Liquids, and Solids in Snow. *Atmospheric Chemistry and Physics*. February 12, 2014, pp 1587–1633. https://doi.org/10.5194/acp-14-1587-2014.

(8) Peters, J. H.; Dette, H. P.; Koop, T. Glyoxal as a Potential Source of Highly Viscous Aerosol Particles. *ACS Earth and Space Chemistry* **2021**, *5* (12), 3324–3337. https://doi.org/10.1021/acsearthspacechem.1c00245.

(9) de Haan, D. O.; Corrigan, A. L.; Smith, K. W.; Stroik, D. R.; Turley, J. J.; Lee, F. E.; Tolbert, M. A.; Jimenez, J. L.; Cordova, K. E.; Ferrell, G. R. Secondary Organic Aerosol-Forming Reactions of Glyoxal with Amino Acids. *Environmental Science and Technology* **2009**, *43* (8), 2818–2824. https://doi.org/10.1021/es803534f.

(10) Shapiro, E. L.; Szprengiel, J.; Sareen, N.; Jen, C. N.; Giordano, M. R.; Mcneill, V. F. *Light-Absorbing Secondary Organic Material Formed by Glyoxal in Aqueous Aerosol Mimics*; 2289; Vol. 9.

(11) Fu, T. M.; Jacob, D. J.; Wittrock, F.; Burrows, J. P.; Vrekoussis, M.; Henze, D. K. Global Budgets of Atmospheric Glyoxal and Methylglyoxal, and Implications for Formation of Secondary Organic Aerosols. *Journal of Geophysical Research Atmospheres* **2008**, *113* (15). https://doi.org/10.1029/2007JD009505.

(12) N. Wren, S.; P. Gordon, B.; A. Valley, N.; E. McWilliams, L.; L. Richmond, G. Hydration, Orientation, and Conformation of Methylglyoxal at the Air–Water Interface. *The Journal of Physical Chemistry A* **2015**, *119* (24), 6391–6403. https://doi.org/10.1021/acs.jpca.5b03555.

(13) Ervens, B.; Turpin, B. J.; Weber, R. J. Secondary Organic Aerosol Formation in Cloud Droplets and Aqueous Particles (AqSOA): A Review of Laboratory, Field and Model Studies. *Atmospheric Chemistry and Physics*. 2011, pp 11069–11102. https://doi.org/10.5194/acp-11-11069-2011.

(14) Gordon, B. P. *EXPERIMENTAL AND COMPUTATIONAL VIBRATIONAL SUM FREQUENCY SPECTROSCOPY STUDIES OF ATMOSPHERIC ORGANICS AND THEIR SURFACE-ACTIVE HYDRATION AND OLIGOMER PRODUCTS AT THE AIR-WATER INTERFACE*; 2019.

(15) Hastings, W. P.; Koehler, C. A.; Bailey, E. L.; de Haan, D. O. Secondary Organic Aerosol Formation by Glyoxal Hydration and Oligomer Formation: Humidity Effects and Equilibrium Shifts during Analysis. *Environmental Science and Technology* **2005**, *39* (22), 8728–8735. https://doi.org/10.1021/es050446l.

(16) Loeffler, K. W.; Koehler, C. A.; Paul, N. M.; de Haan, D. O. Oligomer Formation in Evaporating Aqueous Glyoxal and Methyl Glyoxal Solutions. *Environmental Science and Technology* **2006**, *40* (20), 6318–6323. https://doi.org/10.1021/es060810w.

(17) Avzianova, E.; Brooks, S. D. Raman Spectroscopy of Glyoxal Oligomers in Aqueous Solutions. *Spectrochimica Acta - Part A: Molecular and Biomolecular Spectroscopy* **2013**, *101*, 40–48. https://doi.org/10.1016/j.saa.2012.09.050.

(18) de Haan, D. O.; Corrigan, A. L.; Tolbert, M. A.; Jimenez, J. L.; Wood, S. E.; Turley, J. J. Secondary Organic Aerosol Formation by Self-Reactions of Methylglyoxal and Glyoxal in Evaporating Droplets. *Environmental Science and Technology* **2009**, *43* (21), 8184–8190. https://doi.org/10.1021/es902152t.

(19) Prisle, N. L.; Raatikainen, T.; Laaksonen, A.; Bilde, M. Surfactants in Cloud Droplet Activation: Mixed Organic-Inorganic Particles. *Atmospheric Chemistry and Physics* **2010**, *10* (12), 5663–5683. https://doi.org/10.5194/acp-10-5663-2010.

(20) Lambert, A. G.; Davies, P. B.; Neivandt, D. J. Implementing the Theory of Sum Frequency Generation Vibrational Spectroscopy: A Tutorial Review. *Applied Spectroscopy Reviews* **2005**, *40* (2), 103–145. https://doi.org/10.1081/ASR-200038326.

(21) Yamaguchi, S.; Suzuki, Y.; Nojima, Y.; Otosu, T. Perspective on Sum Frequency Generation Spectroscopy of Ice Surfaces and Interfaces. *Chemical Physics* **2019**, *522*, 199–210. https://doi.org/10.1016/j.chemphys.2019.03.005.

(22) Wei, X.; Miranda, P. B.; Zhang, C.; Shen, Y. R. Sum-Frequency Spectroscopic Studies of Ice Interfaces. *Physical Review B - Condensed Matter and Materials Physics* **2002**, *66* (8), 854011–8540113. https://doi.org/10.1103/PhysRevB.66.085401.

(23) Dreier, L. *Spectroscopic Studies of Water at Charged Interfaces*; 2018.

(24) Asenath-Smith, E.; Hoch, G. R.; Erb, C. T. Adhesion of Freshwater Columnar Ice to Material Surfaces by Crystallization from the Melt. *Journal of Crystal Growth* **2020**, *535*. https://doi.org/10.1016/j.jcrysgro.2020.125563.

(25) Shrestha, P. *Understanding the Interactions of Molecules with Ice*.

(26) Cyran, J. D.; Backus, E. H. G.; van Zadel, M.-J.; Bonn, M. Comparative Adsorption of Acetone on Water and Ice Surfaces. *Angewandte Chemie* **2019**, *131* (11), 3659–3663. https://doi.org/10.1002/ange.201813517.

(27) Hudait, A.; Allen, M. T.; Molinero, V. Sink or Swim: Ions and Organics at the Ice-Air Interface. *J Am Chem Soc* **2017**, *139* (29), 10095–10103. https://doi.org/10.1021/jacs.7b05233.

(28) Zhang, X.; Hoobin, P.; Burgar, I.; Dieu Do, M. Chemical Modification of Wheat Protein-Based Natural Polymers: Cross-Linking Effect on Mechanical Properties and Phase Structures. *Journal of Agricultural and Food Chemistry* **2006**, *54* (26), 9858–9865. https://doi.org/10.1021/jf061597q.